A Buckling Flexure-Based Force-Limiting Mechanism

Jonathan Slocum[1]
MIT,
77 Massachusetts Avenue, Room 3-253,
Cambridge, MA 02139
e-mail: jtslocum@mit.edu

Kenneth Kamrin
MIT,
77 Massachusetts Avenue, Room 1-310,
Cambridge, MA 02139
e-mail: kkamrin@mit.edu

Alexander Slocum
MIT,
77 Massachusetts Avenue, Room 3-461,
Cambridge, MA 02139
e-mail: slocum@mit.edu

A force-limiting buckling flexure has been created which can be used in a wide range of applications where excessive force from an implement can cause harm or damage. The buckling flexure is monolithic, contains no electronics, and can be manufactured using a single shot in an injection molding machine, making it cost effective. In this paper, the design of the flexure is applied to a force-limiting toothbrush as a design study to show its application in a real-world technology. An overview of the buckling flexure is presented, and a structural model is presented to predict when the flexure will elastically buckle. Flexures of different geometries were tested and buckled. The data show that the model can predict buckling of the flexure with an error of 20.84%. A finite element model was also performed which predicts buckling of the flexure within an error of 25.35%. Furthermore, a preliminary model is presented which enables the design of the buckling beam's displacement, such that the total breakaway deformation can be maximized, making sensing the sudden deformation easier to detect. As part of the application of the buckling flexure, an ergonomic, injection moldable toothbrush was created with the flexure built into the neck of the brush. When the user applies too much force while brushing, the flexure gives way and alerts the user when they have applied too much force; when the user lets off the force, the brush snaps back to its original shape. This design methodology is generalized and can be utilized in other force limited applications where an injection-moldable, preset force, and purely mechanical breakaway device is desired. [DOI: 10.1115/1.4043317]

1 Introduction

Force-feedback and force-limitation are essential in sensitive operations such as surgery, handling of foods or produce, processes where people are interacting with robotics, and even dental hygiene [1–4]. In machinery, it is difficult to replicate this force feedback in a reliable and cheap manner without the need to sacrifice speed, simplicity, or productivity. For humans, this force feedback comes naturally and is developed through experience, however in the case of dental hygiene or cosmetics, excessive force can cause irreparable damage to sensitive tissues.

There exist many devices designed to provide this force-limitation or force feedback through sensors, breakaway couplings, or compliant mechanisms. However, these methods either contain several moving parts or require the use of electronics to achieve force limitation [5–21]. This increases both cost and complexity which makes their application in disposable or low-cost devices limited.

In the case of robotic sensing and in MEMs devices, some work has been done on the use of flexures and compliant mechanisms to assist with force-sensing or force-limiting in different applications. The design of a flexural-based tridimensional accelerometer is shown by Gao and Zhang in which they use compliant monolithic flexural hinges in three axes to provide high sensitivity and high resolution [22]. Other force-sensing flexure work done by Wei and Xu present a 1-D force sensor with mN resolution using multiple parallel anti-parasitic motion flexure blades in order to inject cells with high enough accuracy [23]. Zhang et al. present a design of a compound constant-force mechanism in which a parallel double-beam flexure is positioned such that it has zero stiffness over a relatively large stroke [24]. A similar design which helped inspire the design presented in this paper was done by Brenner et al. and Li et al. in which they demonstrate a bistable switch that driven by double and single beam flexures driven by an electrostatic actuator [25,26].

Buckling is also employed for some force-sensing applications. An et al. developed a non-linear buckling sensor which uses a tapered and cantilevered buckling beam for mechanical sensing in seismometers for instance. The cantilevered beam is preloaded to just to buckling and is then slid on a plate. As the beam is preloaded to just around the bifurcation point, it is highly sensitive to changes in motion, thus when the plate moves, the beam will change shape, providing data for sensor output [27]. Buckled shapes are visually used to determine force applied on a nanoscale in work by Dobrokhotov et al. in which a 15.6 μm wire or "needle" is grown and then used to probe nano-fibers and other like-sized structures. Critical buckling loads are used then to determine force applied to these nano-structures [28].

Here, we show a monolithic force-limiting flexure that buckles suddenly when excessive force is applied, but restores to its original shape when the force is relieved. At the point of buckling, there is a sudden change in shape of the flexure and an audible "click" is produced when the buckling beam strikes an anvil, both signals can be used to detect when excessive force is applied. The buckling flexure is monolithic and employs a twin-beam structure with an upper beam that includes a nesting arch on its underside, and a lower buckling beam member which buckles when excessive force is applied to the tip; however, the buckling member (buckling beam) engages the stiffening anvil to form a stiff structure for the user or machine to operate if desired without risk of damaging the flexure or the machine. As the buckling flexure is a single piece, it can be manufactured at a very low cost, making it ideal for applications where devices need force-limitation but are thrown out after a single use. This buckling flexure could also be used in a robotic hand such as one shown by She et al. to provide an upper force-limit sensor to the fingers to if such a feature was desirable [29]. In this paper, the buckling flexure is analyzed and designed into the neck of a toothbrush since excessive force while brushing has been shown to harm dental tissue [4,30,31]. The presented analysis of the flexure is generalized even though it is employed in the neck of a toothbrush, thus it can be applied to design flexures for devices that need cheap and reliable force-limitation.

2 Buckling Flexure Design in a Toothbrush

For this paper, the buckling flexure is designed into the neck of a toothbrush to limit the amount of force a user can exert while brushing. The force-limiting buckling flexure is shown in the neck of a toothbrush in Fig. 1(*a*). The flexure will change state when a critical

[1]Corresponding author.

Contributed by the Mechanisms and Robotics Committee of ASME for publication in the Journal of Mechanisms and Robotics. Manuscript received September 3, 2018; final manuscript received March 20, 2019; published online May 17, 2019. Assoc. Editor: Guimin Chen.

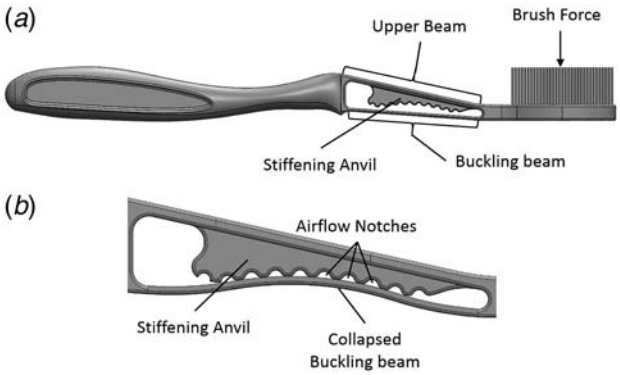

Fig. 1 (*a*) Toothbrush with buckling beam and stiffening anvil to alert users when they are exerting too much force while brushing. (*b*) A close-up of the buckling flexure where the buckled beam is pressing against the stiffening anvil. The anvil serves three purposes: to provide an audible click when the buckling beam strikes, to limit travel (and stress) of the buckled beam, and couple the two beams together to stiffen the structure post-buckling to ensure the device will not plastically deform or break. This protects both the user and the device from harm.

force (in this case from brushing teeth) is exceeded. There are three main elements of the flexure: the upper beam, the buckling beam (which allows the structure to elastically buckle when too much force is applied), and the stiffening anvil. The stiffening anvil is struck by the buckling beam to produce an audible click and prevent plastic deformation after buckling if the user continues to press harder. When the buckling beam and stiffening anvil contact, the structure forms a tighter structural loop than before and stiffens the structure in its post-buckling state. The user brushes their teeth as they normally would and the flexure only buckles as soon as too much force is applied while brushing. Until this point, the brush exhibits normal stiffness.

The buckled shape of the flexure is shown in Fig. 2(*b*)—the stiffening anvil is shaped to fit the shape of the buckling beam after excessive force is applied to the head. The stiffening anvil prevents further travel after buckling, thus maintaining the stiffness of the structure. There is area-contact between the flexure and the anvil in order to reduce the unsupported length of the buckling beam, thus preventing second-order buckling modes from occurring even if further excessive force is applied. During the design process and as models were tested, the area contact was observed to damp the "click" as air and/or fluid was pushed out of the contact; hence the stiffening anvil surface was segmented with a ripple structure and a louder, more discernable click was then obtained when the buckling beam struck the anvil. The inspiration for this design came from the use of helper springs on a trucks and from previous work of anvils used to limit the stroke of a flexible beam in the design of a bistable relay [25,26]. The ridges of the anvil prevent damping of the buckling beam and create a more distinct "snap," which is important in the case of a toothbrush. However, for other systems some firm damping may be desired to reduce impact stresses.

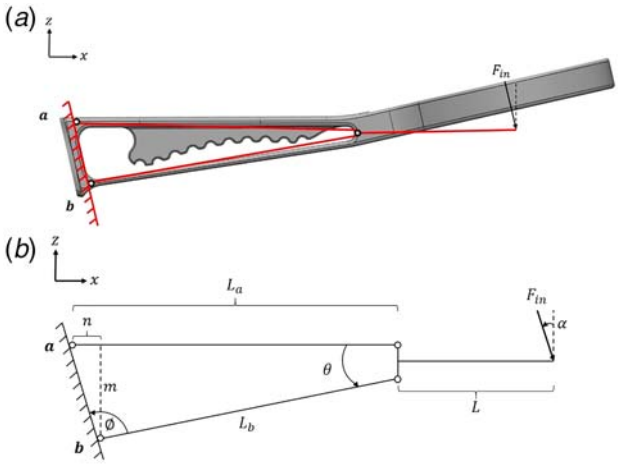

Fig. 2 (*a*) The simplified structure imprinted on the original brush and (*b*) the structure with labeled dimensions and angles used in the following analysis as well as a free-body diagram of the structure with resultant forces. Note that F_{in} has been broken into its *x*–*y* vector components F_1 and F_2.

3 Analysis

3.1 Analytical Buckling Model. For modeling simplicity, the stiffness of the upper member is considered very large in comparison to the connecting nodes. Figure 2(*a*) shows a simplified structure of the structure imprinted onto the neck of the toothbrush. Figure 2(*b*) is the free body diagram of the structure with labeled dimensions and angles that are relevant to the development of an analytical model. For clarification, the segment $L_a + L$ is a continuous and treated as rigid as well. The handle is treated as a rigid structure, for the force analysis only to determine the critical buckling load. The top beam is a single entity, which includes the upper beam (L_a). The buckling beam (L_b) is treated as a two force member for simplicity, thus the structure acts as a quasi-truss for the buckling load analysis.

To analyze how this structure will fail, the upper beam (L_a) and buckling beam (L_b) are connected with pin joints. It is assumed that the force (F_{in}) is applied in the middle of the bristles as a point load, which is at a small angle to the buckling beam. The goal of this model is to resolve the axial forces inside the buckling beam (F_b) and upper beam (F_a) as a function of the applied force and the geometry of the structure. From this the buckling beam can be sized to buckle under a given compressive load, driven by the applied force.

An input normal force F_{in} from brushing creates two resultant force components F_1 and F_2 at the head of the brush where the bristles are. Resultant forces act at points *a* and *b* on the geometry shown in Fig. 2(*c*); equilibrium equations were generated (Eqs. (1)–(3)) resulting in three equations and four unknowns (F_{ax}, F_{bx}, F_{az}, F_{bz}). It is important to note that the boundary conditions for the beams are assumed pinned and the internal moments thus negligible. In reality the molded plastic brush would have moment connections, not pin joints, but because of slender beams and connections, this simplification proves justified in order to develop a first-order design analysis tool:

$$\sum F_x = 0 = F_2 + F_{ax} + F_{bx} \tag{1}$$

$$\sum F_z = 0 = F_1 + F_{az} + F_{bz} \tag{2}$$

$$\sum M_{ya} = 0 = -F_1(L_a + L) + F_{bx}c \tag{3}$$

The force in L_b is axial, so it can be related to vector components using nodal analysis (Eq. (4)). Thus, F_{bx} can be expressed as a function of the angle θ of the buckling beam and the axial force in L_b (F_b). A new sum of moments is expressed in terms of the internal axial force (F_b) of the buckling beam L_b in Eq. (5).

$$F_b = \frac{F_{bx}}{\cos\theta} \tag{4}$$

$$\sum M_{ya} = 0 = F_b c \cdot \cos(\theta) - F_1(L_a + L) \tag{5}$$

Using Eq. (5), the axial force F_b in the buckling beam (L_b) can be expressed as a function of the input force and the structure geometry (Eq. (6))

$$F_b = \frac{F_{in}(L_a + L)\cos\alpha}{c \cdot \cos(\theta)} \tag{6}$$

Equation (6) yields an expression for the axial force in the buckling beam as a function of the known input forces F_1 and F_2, and the known geometry. The goal is to determine what input force F_{in} (which is a function of F_1 and F_2) will cause the structure to buckle; to do this F_b is defined to be equal to the critical buckling load of the buckling. Recall from Fig. 1(*b*) that the shape of the collapsed buckling beam is a cosine function. Since this beam is long and slender (slenderness ratio for all beam variations $\lambda >$ 270), an Euler buckling model can be used. In order to create a cosine-shape of the buckling beam using the Euler model, clamped–clamped boundary conditions must be assumed. In our model this provides the lower bound of the buckling force, and the condition for buckling in the flexure can be expressed as F_b being greater than or equal to the calculated buckling load as predicted by the Euler model (Eq. (7))

$$F_{b-buckle} \geq \frac{\pi^2 EI_b}{4L^2} \tag{7}$$

The known minimum value of F_b from Eq. (7) enables calculation of a maximum input force F_{in-max} by relating F_1 and F_2 (Eq. (8*a*)), and using only geometric parameters of the beam. These parameters can now be adjusted to reach the critical brushing force desired. For the sake of a sensitivity analysis, the cosine term in Eq. (8*a*) is expressed as a function physical dimensions of the flexure L_a and c, respectively, shown in Eq. (8*b*)

$$F_{in-max} = \frac{\dfrac{\pi^2 EI_b}{4L^2}(c\cos\theta)}{\cos\alpha(L + L_a)} \tag{8a}$$

$$F_{in-max} = \frac{\pi^2 EI_b}{4\cos\alpha} \frac{c\left(\dfrac{L_a}{\sqrt{L_a^2 + c^2}}\right)}{L^2(L + L_a)} \tag{8b}$$

In order to determine which variables have the largest effect on buckling force, a sensitivity analysis of Eq. (8*b*) is done by taking the Jacobian with respect to physical measured dimensions c, L, and L_a. Physical parameters from test flexures shown later in the paper were used with the partial derivatives to reveal the most sensitive parameters

$$\frac{\partial F_{in-max}}{\partial L} = \frac{\pi^2 EI_b}{4\cos\alpha} \frac{cL_a(2L_a + 3L)}{L^3\sqrt{c^2 + L_a^2}(L_a + L)^2} = 0.14 \tag{9a}$$

$$\frac{\partial F_{in-max}}{\partial L_a} = \frac{\pi^2 EI_b}{4\cos\alpha} \frac{c(c^2 L - L_a^3)}{L^2(c^2 + L_a^2)^{3/2}(L_a + L)^2} = -0.02 \tag{9b}$$

$$\frac{\partial F_{in-max}}{\partial c} = \frac{\pi^2 EI_b}{4\cos\alpha} \frac{L_a^3}{L^2(c^2 + L_a^2)^{3/2}(L_a + L)} = 0.20 \tag{9c}$$

Results of the Jacobian show that the critical buckling load (Eq. (8*a*) or Eq. (8*b*)) is most sensitive to c, which is the distance between the two nodes a and b (the distance between the upper beam and the buckling beam).

3.2 Analytical Buckling Model. Shown so far is a predictive model when the structure will fail. The next step is to calculate when the structure will yield, or rather calculate the maximum lateral displacement of the buckling beam so as to maximize the disturbance caused when too much force is applied. Though the model used to estimate the buckling force assumes a pinned–pinned boundary condition for the buckling beam, the actual shape resembles a sinusoid, which is indicative of clamped–clamped boundary conditions. To start, the stress at buckling can be calculated for any clamped–clamped slender beam using Eq. (10) where r is the radius of gyration of the structure

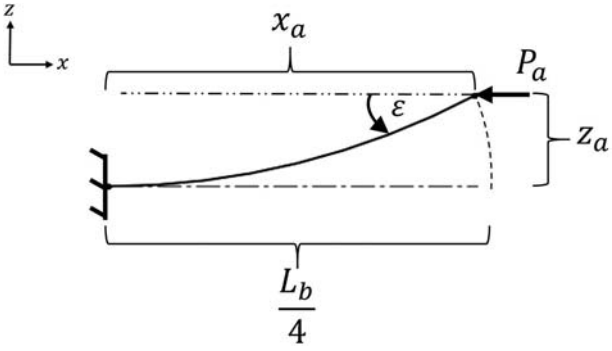

Fig. 3 Large deflection of a slender buckled column with clamped and free end boundary conditions, respectively. This represents one-fourth of the total length of the buckling beam shape.

$$\sigma_{cr} = \pi^2 E\left(\frac{2r}{l_{ef}}\right)^2 \tag{10}$$

Solving for lateral displacement of buckled columns is well documented in Timoshenko's "Theory of Elastic Stability" [32], where the primary example is a clamped beam with a free, unsupported end subjected to a point load (Fig. 3). This column represents a quarter of a buckled column that has clamped–clamped boundary conditions, thus the total length of the column here has been adjusted to a quarter of the buckling beam length.

Since the buckling beam deforms in the shape of a cosine function (Fig. 4)—the goal is to determine the magnitude of this function, as the shape is already assumed. From this, we can approximate the internal moment using the basic beam theory.

The shape of the function in Fig. 4 is shown in Eq. (11). Timoshenko derives effectively half the magnitude k of this deflection numerically by using the given geometry of the beam and solving for the deformed lengths using elliptical integrals. These integrals have already solved numerical solutions which Timoshenko displays values for the deformed magnitudes (Table 1).

$$u(x) = k\left(1 - \cos\left(\frac{2\pi x}{L}\right)\right) \tag{11}$$

Thus, if the buckling beam was buckled to 20 deg at its inflection point, using Table 1 and the length of the buckling beam L_b the peak deflection would be 18.3 mm. It is important to note that this is significantly larger than any neck for any toothbrush. Thus, this serves as an upper limit to what the flexure would ever need to be deformed to. This value is the magnitude k of the deformed shape of the deflection so the internal moment can

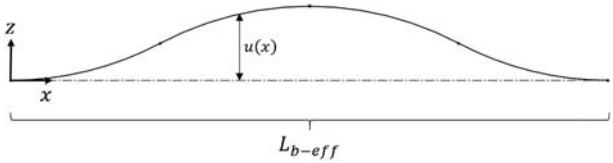

Fig. 4 Deformed shape of the buckling beam—note that it is the shape of a cosine function

Table 1 Values of the deformed shape for a given angle at the inflection point of the cosine function. This table has been adjusted from Timoshenko's original work to fit the current buckling beam. Note that F_{b-crit} is the minimum force required to buckle the buckling beam.

ε	20 deg	40 deg	60 deg
$\frac{F_{in}}{F_{b-crit}}$	1.015	1.063	1.152
$\frac{x_a}{(L_b/2)}$	1.94	1.762	1.482
$\frac{y_a}{(L_b/2)}$	0.440	0.844	1.186

be approximated by differentiating the deflection (Eq. (12))

$$M(x) = -\frac{4\pi^2 k}{L_b^2}\cos\left(\frac{2\pi x}{L_b}\right) \tag{12}$$

From this function, the maximum moment occurs at the clamped ends and in the middle of the beam. Thus, the maximum bending stress (Eq. (13)) can be solved using Eq. (12), where t_{beam} is the thickness of the buckling beam and I_b is the area moment inertia of the buckling beam

$$\sigma_{max-buckle} = \frac{M_{max} t_{beam}}{2I_b} \tag{13}$$

The total stress inside the beam does not increase by more than 0.5 MPa for the thinnest structure, which is shown in Table 1 as a very small load increase will result in a large increase in deflection of the buckled shape. To compare, the stress in the upper beam can be compared to the stress in the buckling beam. The stress in the upper beam can be approximated using deflection at the point where F_{in} is applied. Thus, a cantilevered beam model can be employed since the stress in the upper beam is only dependent on the deflection it has undergone. The force can be found as a function of the deflection and geometry (Eq. (14)), where δ_{tip} is the maximum deflection in the beam

$$F_{cantilever} = \frac{3\delta_{tip} E I_a}{(L + L_a)^3} \tag{14}$$

The maximum moment for a cantilever occurs at the base of the beam, thus the maximum stress experience by the upper beam can be calculated (Eq. (15)). The stress shown here will be used to compare to the buckling stress computed in the results section

$$\sigma_{max-a} = \frac{F_{cantilever}(L_a + L)t_a}{2I_a} \tag{15}$$

4 Methods

4.1 Analytical Buckling Model. Test flexures were cut with an abrasive water jet[2] from 6.25 mm thick scratch-resistant polycarbonate (Fig. 5); polycarbonate exhibits good elastic properties, minimizing hysteresis effects when the structure recovers from the buckled state. It is also similar in modulus to styrene-acrylonitrile, which is commonly used in manufacturing manual toothbrushes. Styrene-acrylonitrile is not readily available for manufacture of prototypes; thus it was more practical to use polycarbonate as a substitute. Six total samples were cut with buckling beam thicknesses varying from 0.9 mm to 1.35 mm to assess the validity and accuracy of the analytical model. These were the only thicknesses tested as the force required to buckle the flexures was within the reasonable range for a potential force-limiting toothbrush, which is less than 6–7 N of force. Samples were also cut using representative dimensions for a standard toothbrush. Iterative testing was performed to determine brush geometries that yielded buckling forces due to brushing between 1 and 5 N of force.

[2]OMAX MICROMAX Precision Jet Machining Center: https://www.omax.com/omax-waterjet/micromax

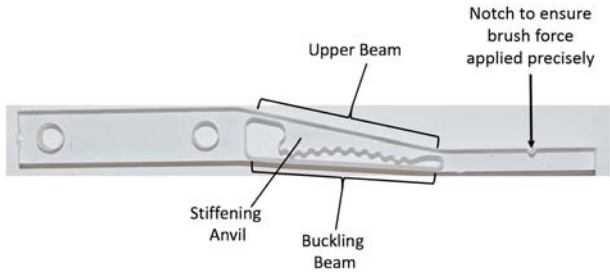

Fig. 5 A test buckling flexure cut from polycarbonate. Mounting holes allow the flexure to be clamped securely for force displacement testing. A notch was created at a known distance from the flexure to ensure samples were repeatedly tested in the same position.

Test flexures with different buckling beam thicknesses were mounted in a fixed testing mount shown in Fig. 6, and then deformed with an actuated load cell until the buckling beam completely conformed to the stiffening anvil. Samples were tested in an Admet Universal Testing Machine using a 2.2lbf 600 Series Overload-Protected S-Bend Load cell. The Admet Testing Machine has a positional accuracy of ±0.01 mm and the load cell was calibrated to ±0.001 N. The testing machine pushed perpendicular to the notch of each beam of the flexure until the buckling beam conformed to the arch structure. This is the moment at which a user would likely stop brushing—all brush samples were pushed with at least 5 N of force before the load cell was retracted. Pushing harder than the buckling force verified the design intent to have the buckled beam effectively connect with the upper beam by contact with the anvil.

4.2 Finite Element Model. Finite element model (FEM) of the tested flexures was also generated for comparison of critical buckling loads. Solid models of each test flexure were generated for each test flexure. SolidWorks buckling simulation was used to find critical loads of each of the test flexures (Fig. 7). To determine the critical buckling load in SolidWorks simulation, the model was given clamped fixtures at the bolt holes meant for the real test flexures. The finest mesh size was selected in the program as the simulation

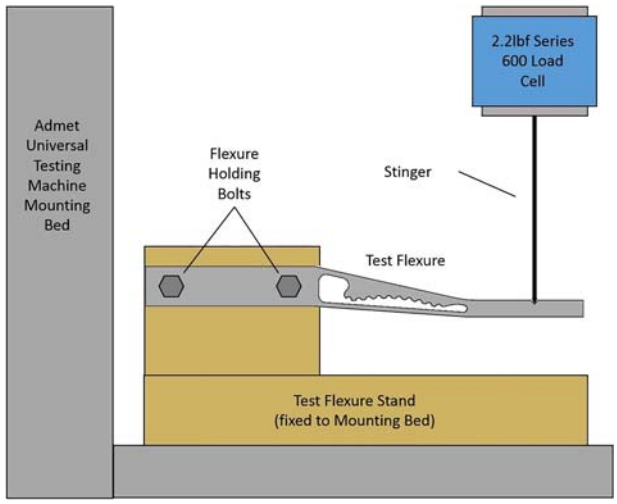

Fig. 6 Test setup to deform the polycarbonate testing flexures. Three main components allow the force–displacement of the buckling flexure to be measured: the testing flexure itself, a fixed testing mount, and an actuated load cell.

Fig. 7 Solid model of one of the test flexures showing the constraints and loads used for the finite element analysis and the mesh used for the buckling simulation. The test flexures were clamped at the bolt holes and the force was applied at the same notch that was used for the real measurements of the test flexures.

did not take longer than a minute to run. A test load of 1 N was applied to the tip of the test flexures. Once the simulation was performed, it provided a load factor to relate to 1 N of load. The critical buckling load, according to the simulation, is the applied load (1 N in this case) multiplied by the load factor. The Appendix has the FEM simulation results that were conducted using SolidWorks.

5 Results

Since the moduli of polymers can vary depending on the batch of material that is used, the modulus of elasticity was measured by buckling against a scale a long, slender column (slenderness of 360) of material cut from the same stock as was used for the test flexures. A pinned–pinned Euler buckling model was used (Eq. (16)). The average modulus for the polycarbonate from which the prototypes were cut was measured to be 2.58 ± 0.03 GPa. A single beam was tested and 13 different measurements were taken

$$E = \frac{F_{measure} L^2}{\pi^2 I} \tag{16}$$

Force–displacement data were collected using the setup shown in Fig. 6. Buckling flexures with different buckling beam thicknesses were mounted and deformed past buckling. The distance between the stiffening anvil and the buckling beam was also kept constant so that the buckling beams across all variations would have the same travel as they were deformed and buckled. Since the waterjet cutter produces a small taper when it cuts, the buckling beam thicknesses on test flexures were measured along five positions on both sides of the thickness approximately evenly spaced. Measured thickness values were used to generate an average thickness of the buckling beam which is presented in Fig. 8. These data were plotted against one another to show how the critical load of the flexure increases as the buckling beam thickness increases (Fig. 8). The error of data in Fig. 8 is limited to the resolution of the testing stage and load cell used. The Admet machine has repeatability to ±0.01 mm and the load cell was calibrated to ±0.001 N. For these

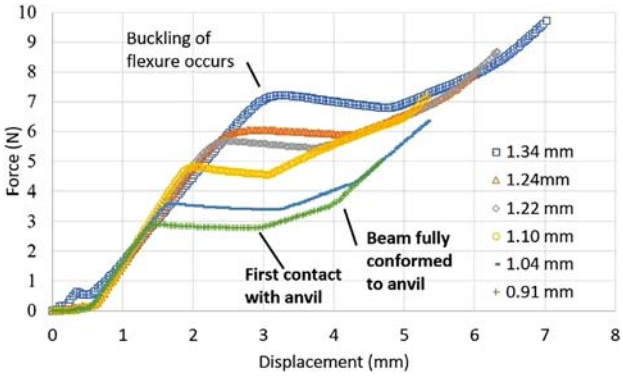

Fig. 8 Force–displacement data for test flexures with different buckling beam thicknesses. Only one set of flexures with each thickness was measured. As beam thickness increases, the critical buckling load (first peak in the plots) of the structure also increases. Once the buckling beam conforms to the anvil, the structure stiffens again, as shown by the change of slope after approximately 3 mm of displacement.

data, error bars of the points in Fig. 8 were left out as they cluttered the image and obscured valuable information about the structure.

For all six different test flexures, as the force applied increases, they undergo a linear elastic regime for approximately 1–3 mm of displacement depending on the thickness of the buckling beam. Once the critical load has been reached, the stiffness rapidly changes as the buckling beam buckles and starts to snap through toward contact with the stiffening anvil. After buckling, the structure goes through a period of near zero or negative stiffness for about 1–2 mm of stroke until the stiffening anvil is contacted. Once the stiffening anvil is contacted, positive stiffness is then restored to the structure. As the buckling beam fully conforms to the stiffening anvil, there is a sudden increase in stiffness as the structural loop is completed and the test flexure acts as a homogenous structure.

The first peak is when the buckling beam buckles—this is the critical buckling load, shown as the measured input force in Table 2. After buckling, the buckling beam strikes and mates with the stiffening arch of the upper beam. This measured critical load was compared to the predicted critical loads calculated using the previously derived model—these values are shown in Table 2. The finite element model is also shown for comparison to the measured values. The total average error across all beam thicknesses between the measured input force and the predicted input force that was calculated using Eq. (8) is 20.84%. The FEM model predicted higher than average critical buckling loads than the measured amounts by an average of 25.35% (see the Appendix for the FEM model simulation results). Thus, the measured values are bounded between the analytical model and the FEM model predicted critical buckling loads.

The stress at buckling in the buckling beam for the flexures tested was calculated assuming an approximate yield of 60 MPa for polycarbonate (Table 3) using equation. With respect to the upper beam —the maximum stress sustained from 6 mm of deflection (approximately the largest deflection all test samples underwent) is 34 MPa using Eq. (15).

To determine the feasibility of the force-limiting structure in a real toothbrush, a buckling flexure was designed and printed to fit with a replaceable brush head and a compact travel toothbrush

Table 2 Buckling beam thicknesses and the corresponding measured input force and predicted force values. As the beam gets thicker, the total amount of the model error decreases. The average analytical model error is 20.84% and the average FEM model error is 25.35%.

Buckling beam thickness (mm)	Measured input force (N)	Analytical model predicted force (N)	FEM predicted force (N)	Analytical model error (%)
0.91	2.83	2.07	3.19	26.74%
1.04	3.52	3.15	4.70	13.30%
1.10	4.69	3.67	5.40	35.75%
1.22	5.54	5.08	7.26	16.03%
1.24	5.91	5.27	7.50	22.43%
1.34	7.04	6.73	9.35	10.78%

Table 3 Approximate stress inside the flexure beams at buckling. All the columns are considered slender columns.

Buckling beam thickness (mm)	Slenderness ratio	Buckling stress (MPa)	% of yield stress
0.905	80	4.00	5.00
1.04	69	5.28	6.60
1.095	66	5.85	7.32
1.22	59	7.27	9.08
1.235	58	7.44	9.31
1.34	54	8.76	10.96

Fig. 9 Sample buckling flexure designed to mate with a removable handle and toothbrush head. This flexure can be used for brushing and can be compactly stored.

handle (Fig. 9). The buckling beam was tapered under than the anvil to help prevent pinching of any tissue inside the mouth when the flexure buckles. As the buckling beam is tapered, the force to buckle it decreases linearly with the width. As the buckling force goes with the cube of the thickness, only a small increase in thickness is needed to accommodate of a moderate change in width of the buckling beam.

6 Discussion

The analytical model presented can predict the measured buckling load of the structure with an average 20.84% error across all beam thicknesses tested. For comparison, the FEM model can predict the critical buckling load of the structure with an average error of 25.35%. The FEM model predicted higher critical loads as the stiffness of the upper beam may be playing a more significant role in the model than it should, or it assumes the bending moments at the end of the buckling beam are not as significant relative to the moment needed to deform the upper beam. Both models bound the measured data, where the FEM model is above the measured critical load, and analytical model is below it. Thus, both methods can be used to predict the critical load of the flexure to within reasonable accuracy, however averaging the two results may give an even more accurate result as the average will often be closer to the measured critical load.

The analytical model assumes the structure is comprised of two-force members, which do not include any resistive bending moments of the actual flexure elements. In actuality, the flexure deforms slightly and the upper beam does experience some bending that acts as an additional spring. This perhaps explains why the predicted input force for buckling the structure is lower than the actual measured amount. Indeed, what is not included in the model is the presence of an internal moment in the buckling beam, which would make it behave like an imperfect column. Since the beam has clamped–clamped boundary conditions and the input force creates an applied moment on the structure, the column will require less force to buckle than if a single compressive force were applied. Both assumptions are potentially offsetting in the calculation; the top beam acts as a resistive spring that increases the buckling load of the buckling beam as it must also be deformed in order for buckling to occur. The resulting internal moment of the buckling beam due to the boundary conditions would lower the critical buckling load, thus the effects of the upper beam stiffness and the lower beam internal moments act against one another. The simplified model presented here appears to be accurate enough to design the system and study how changes in various parameters buckling forces. In addition, the polymer itself is inherently a viscoelastic material, so thinner beams likely have increased variance in terms of their mechanical properties across the thickness of the beam.

In order to further validate the flexure, material and longevity testing will need to be done. If the flexure is to be used in a toothbrush where repeated buckling may be observed, fatigue and eventual failure of the flexure must be analyzed and accounted for so that it will not fail during use and potentially hurt someone. Polycarbonate was selected as the test flexure material as it is readily available and has desirable elastic properties for a plastic. However, if this flexure is to be used in a food-safe product such as a toothbrush other plastics much be used. Styrene acrylonitrile is one potential suitor as it is a relatively elastic polymer and commonly used to make toothbrushes today. Further work must also be done on aging of the plastic and how it affects the critical buckling load. With respect to temperature, for dental applications, the mouth is not much warmer than room temperature. However, if the application of this flexure needs higher temperatures, further testing must be done of plastic flexures at higher temperatures to see how it influences critical buckling load or other materials must be used to achieve the desired effect.

Protecting the buckling beam and flexure structure during operation is an important feature—Fig. 8 shows that the buckling beam strikes the stiffening anvil after buckling, which re-stiffens the structure. Thus, if a user has buckled the structure and continues to press with increasing force, the mechanism is able to protect the user from causing failure of the structure as well as injury to the user. The stiffening anvil also exists as an actual anvil for the buckling beam to strike, creating an audible signal that the structure has deformed and the peak brushing force has been reached.

In the case of a toothbrush the data show that this structure will give way when less than 3 N of force is applied, which is within the 1–4 N threshold found to effectively remove plaque from teeth. What is not quantified in this study is how abruptly the structure buckles (buckling velocity) or any lateral displacement of the buckling beam. It also does not account for the dynamic movements associated with brushing and how the structure will respond while being used. For instance, lateral forces could also have an effect on buckling the flexure, if a compressive lateral force is applied to the structure as well a vertical brushing force (accounted for in the model) are applied, the flexure will likely buckle at a lower brushing force than is demonstrated in this paper. Further testing is warranted to evaluate these buckling modes.

7 Conclusion

A design for a buckling flexure for limiting applied forces has been presented where the flexure uses the principle of self-help to stiffen and strengthen after buckling to prevent damage. Design equations were developed into a predictive model to allow for sizing of members and studying effects of tolerances on performance. The buckling flexure design is demonstrated in a toothbrush handle as a force-limiter to improve a person's ability to properly care for their teeth and gums. Exemplar flexure designs were tested and buckled with critical loads ranging from 2.83 N to 7.04 N achieved by changing only the thickness of the lower buckling beam. The predictive model, with an error of 20.84% below the measured critical load and the finite element model with an error of 25.35% above the measured critical load, can be used to tune the mechanism to the desired stiffness and deterministically set tolerances for manufacture for applications outside the realm of dental hygiene. This design is monolithic, meaning that it can be injection molded in a single shot with no side pulls required. The use of the buckling flexure as a force-limiting device has use in other applications outside of toothbrushes, where excessive force can be damaging such as surgical tools, food-product handling robots, and human-interactive robots. The low-cost and simplicity of the design make it ideal for applications where the product is single use or needs to be low-cost in order to be competitive.

Nomenclature

a = upper beam node
b = buckling beam node
c = distance between node a and b
k = constant derived from elliptical integral
E = modulus of elasticity
L = distance from brush head to flexure
t_{beam} = thickness of buckling beam
l_{b-eff} = effective length of buckled beam
z_a = lateral displacement of buckled beam
F_{ax} = x-direction reaction force at a

F_{az} = z-direction reaction force at a
F_{bx} = x-direction reaction force at b
F_{bz} = z-direction reaction force at b
F_{in} = input force from user
I_a = moment of Inertia of upper beam
I_b = moment of inertia of buckling beam
L_a = upper beam length
L_b = buckling (lower) beam length
P_a = load on buckled shape (F_b is used)
α = angle of input force on structure
δ_{tip} = maximum deflection of cantilever beam approximation
ε = slope at inflection point of buckled shape
θ = angle between L_a and L_b
λ = slenderness ratio
σ_{max} = max bending stress beam

Appendix: Finite Element Models and Testing Setup

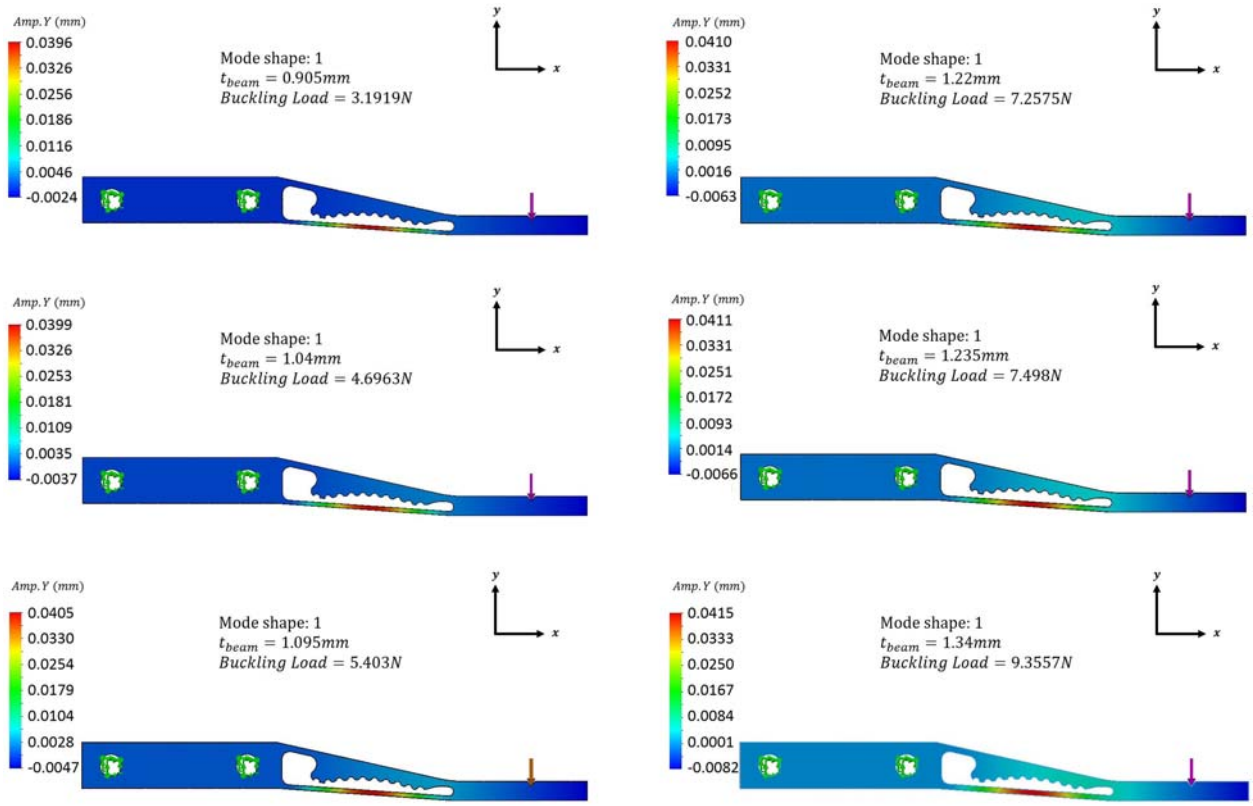

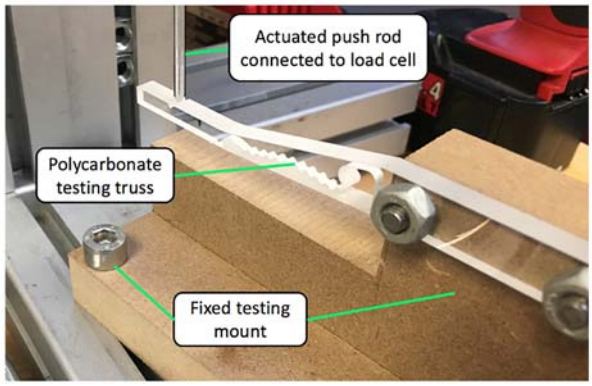

References

[1] Krüger, J., Lien, T. K., and Verl, A., 2009, "Cooperation of Human and Machines in Assembly Lines," CIRP Ann.—Manuf. Technol., **58**(2), pp. 628–646.
[2] De Santis, A., Siciliano, B., De Luca, A., and Bicchi, A., 2008, "An Atlas of Physical Human-Robot Interaction," Mech. Mach. Theory, **43**(3), pp. 253–270.
[3] Zhang, M., Laliberté, T., and Gosselin, C., 2017, "Design and Static Analysis of Elastic Force and Torque Limiting Devices for Safe Physical Human–Robot Interaction," J. Mech. Robot., **9**(2), p. 021003.
[4] Canadian Dental Hygienists Association, 2006, "CDHA Position Paper on Tooth Brushing/Déclaration de L'ACHD Sur Le Brossage Des Dents," Can. J. Dent. Hyg., **40**(5), pp. 1–14. https://www.cdha.ca/pdfs/Profession/Resources/tooth_brushing_paper_reprint.pdf
[5] White, L., and Ingels, L., 1984, "Pressure Sensing Device for Holding a Toothbrush," U.S. Patent No. 4,476,604.
[6] Dirksing, R., 1992, "Toothbrush Having Handle Joined to Brush Head by Non-Pinching Flexible Twin Beam Structure," U.S. Patent No. 5,105,499.
[7] Piserchio, R., 2011, "Pressure-Sensitive Toothbrush," U.S. Patent No. 20110016651A1.

[8] Irizarry, J., 1994, "Pressure Alarm Toothbrush Assembly," U.S. Patent No. 5,331,707.
[9] Craig, J. J., 1981, "Hybrid Position/Force Control of Manipulators," J. Dyn. Syst. Meas. Control, **103**(2), pp. 126–133.
[10] Daniel, E. W., 1977, "Force Feedback Control of Manipulator Fine Motions," J. Dyn. Syst. Meas. Control, **99**(2), pp. 91–97.
[11] Rosenberg, L. B., and Jackson, B. G., 2002, "Force Feedback Device Including Flexure Member Between Actuator and User Object," U.S. Patent No. 6,437,771.
[12] Das, H., Ohm, T. R., and Steele, R. D., 2002, "Tool Actuation and Force Feedback On Robot-Assisted Microsurgery System," U.S. Patent No. 6,385,509.
[13] Pierrot, F., Dombre, E., Dégoulange, E., Urbain, L., Caron, P., Boudet, S., Gariépy, J., and Mégnien, J. L., 1999, "Hippocrate: A Safe Robot Arm for Medical Applications With Force Feedback," Med. Image Anal., **3**(3), pp. 285–300.
[14] Kramer, H., 2001, "Toothbrush Comprising a Flexibly Linked Region in the Head," U.S. Patent No. 6,185,779.
[15] Jungnickel, U., Altmann, N., and Guebler, R., 2014, "Force Sensing Oral Care Instrument," U.S. Patent No. 8,832,895.
[16] Fox, R., Hippen, J., Knaub, D., Resuello, I., Frank, P., and Moskovich, R., 2003, "Replaceable Head Toothbrush Providing Controlled Brushing Pressure," U.S. Patent No. 6,502,272.
[17] Giuliani, D., McMahon, R. W., and McInnes, C., 1998, "Toothbrush With Adaptive Load Sensor," U.S. Patent No. 5,784,742.
[18] Huefner, N. F., and Burrell, F. J., 1994, "Toothbrush Having Adjustable Brushing Pressure," U.S. Patent No. 5,315,732.
[19] Heinzelman, B. D., Lamond, D. R., and Fontayne, D., 1998, "Resiliently Flexible Toothbrush," U.S. Patent No. 5,735,012.
[20] Sundius, C. L., and Mcfadden, B. P., 1999, "Pressure Sensing Toothbrush," U.S. Patent No. 5,876,207.
[21] Mierau, H.-D., and Spindler, T., 1987, "Toothbrush," U.S. Patent No. 4,698,869.
[22] Gao, Z., and Zhang, D., 2012, "Flexure Parallel Mechanism: Configuration and Performance Improvement of a Compact Acceleration Sensor," J. Mech. Robot., **4**(3), p. 031002.
[23] Wei, Y., and Xu, Q., 2016, "Design of a Force Sensor Based on Flexure Beams With Piezoresistive and PVDF Elements," Proceedings of the ASME 2016 International Design Engineering Technical Conferences and Computers and Information in Engineering Conference, Charlotte, NC, Aug. 21–24, pp. 1–7.
[24] Zhang, X., Wang, G., and Xu, Q., 2018, "Design, Analysis and Testing of a New Compliant Compound Constant-Force Mechanism," Actuators, **7**(4), p. 65.
[25] Brenner, M. P., Lang, J. H., Li, J., Qiu, J., and Slocum, A. H., 2003, "Optimal Design of a Bistable Switch," Proc. Natl. Acad. Sci. U.S.A., **100**(17), pp. 9663–9667.
[26] Li, J., Brenner, M. P., Christen, T., Kotilainen, M. S., Lang, J. H., and Slocum, A. H., 2005, "Deep-Reactive Ion-Etched Compliant Starting Zone Electrostatic Zipping Actuators," J. Microelectromech. Syst., **14**(6), pp. 1283–1297.
[27] An, S., Kim, B., Kwon, S., Moon, G., Lee, M., and Jhe, W., 2018, "Bifurcation-Enhanced Ultrahigh Sensitivity of a Buckled Cantilever," Proc. Natl. Acad. Sci. U.S.A., **115**(12), pp. 2884–2889.
[28] Dobrokhotov, V. V., Yazdanpanah, M. M., Pabba, S., Safir, A., and Cohn, R. W., 2008, "Visual Force Sensing With Flexible Nanowire Buckling Springs," Nanotechnology, **19**(3), p. 035502.
[29] She, Y., Li, C., Cleary, J., and Su, H.-J., 2015, "Design and Fabrication of a Soft Robotic Hand With Embedded Actuators and Sensors," J. Mech. Robot., **7**(2), p. 021007.
[30] Rosema, N. A. M., Adam, R., Grender, J. M., Van der Sluijs, E., Supranoto, S. C., and Van der Weijden, G. A., 2014, "Gingival Abrasion and Recession in Manual and Oscillating-Rotating Power Brush Users," Int. J. Dent. Hyg., **12**(4), pp. 257–266.
[31] Löe, H., 2000, "Oral Hygiene in the Prevention of Caries and Periodontal Disease," Int. Dent. J., **50**(3), pp. 129–139.
[32] Timoshenko, S., 1936, *Theory of Elastic Stability*, McGraw-Hill Book Company Inc., New York.